DRAFT 6/5/91

Differential Geometry and the Forming of Aligned Fiber Composites

T. Gutowski, D. Hoult, G. Dillon and J. Gonzalez-Zagusti
Massachusetts Institute of Technology
Cambridge, MA. 02139

Prepared for "Flow Processes in Composite Materials", Limerick, July 1991

1. INTRODUCTION

The forming of aligned fiber composites into complex shapes is a relatively new, and poorly understood, manufacturing process. Nevertheless, it is considerably simpler to understand than many other forming processes. This is because the constraints imposed by the material are so severe that many important problems can be solved by geometric reasoning alone. This was pointed out by Pipkin and Rogers for in-plane deformations of aligned fiber composites [1,2], and Tschebycheff used this idea to show how cloth deforms to a complex surface [3]. In a previous publication we developed this idea for the formation of complex shapes from aligned continuous fiber sheets [4].

Formation of a thin sheet of aligned fibers into an ideal complex shape (i.e. with constant fiber spacing and sheet thickness) is essentially a mapping problem. Once the first fiber is placed, the location of the remaining fibers is determined. The formation process is possible if one can construct what is called a "geodesic set".

In the next section, Section 2, the theory of the mapping process is presented. Section 3 describes a powerful computer algorithm for generating fiber maps, and the three types of singularities which arise. Section 4 shows the experimental results showing broad similarity with theory, and specific correlations between shear the difficulty in forming the part. Section 5 gives the conclusions of this work.

2. THEORY

Consider the surface $\hat{x} = (x, y, z) = \hat{x}(u, v)$. Let $\hat{N}$ be the normal to the surface. As

$$\hat{N} = \frac{\hat{x}_u \times \hat{x}_v}{|\hat{x}_u \times \hat{x}_v|} . \tag{1}$$

where $\hat{x}_u = \frac{\partial \hat{x}}{\partial u}$, when $\hat{N}$ exists u and v are independent.

Choose v = const. to be the fiber paths; the u is normal to the fiber path. See Fig. 1.

With ideal fiber alignment, the fibers are equally spaced, and

$$\hat{x}_u \cdot \hat{x}_u = E = 1 , \tag{2}$$

From orthogonality

$$\hat{x}_u \cdot \hat{x}_v = F = 0 . \tag{3}$$

The arc length along the surface can then be written as

$$ds^2 = du^2 + G(u,v)dv^2 \tag{4}$$

where $G = \hat{x}_v \cdot \hat{x}_v$. This is the standard form for a "geodesic set".

Following standard theory [4], the geodesic curvature is

$$\kappa_g(\text{fibers}) = \frac{1}{2G} \frac{\partial G}{\partial u} . \tag{5}$$

The geodesic curvature for the normal lines (along u directions, or v = const.) is, then

$$\kappa_g(\text{normals}) = - \frac{1}{2E\sqrt{G}} \frac{\partial E}{\partial v} , \tag{6}$$

For an ideal fiber map, E = const, so κ_g(normals) = 0. The normal lines are geodesics.

Consider the deformation of an aligned fiber composite into a curved surface. The in-plane shear can be defined as,

$$d\Gamma_{12} \equiv \frac{ds_1 - ds_0}{du} . \tag{7}$$

Substituting eq. (4) expanding and simplifying yields,

$$d\Gamma_{12} = \frac{1}{2\sqrt{G}} \frac{\partial G}{\partial u} \, dv \, . \tag{8}$$

Hence the shear is related to the geodesic curvature [3,5]. We can now integrate along a fiber, of length L, to find

$$\Gamma_{12} = \int_0^L \kappa_g(s) ds + \Gamma_{12(0)} \, . \tag{9}$$

The constant $\Gamma_{12}(0)$ allows for a constant shear along the entire length of the fiber.

It is helpful to recall the Gauss-Bonnet theorem [4] when evaluating the integral in eq. (9):

$$\int_c \kappa_g \, ds + \int \int_A K dA = 2\pi - \Sigma\theta_i \, . \tag{10}$$

Here K is the "Gaussian curvature", which is the product of the two principal curvatures for the surface at a point. The angles θ_i are defined in the accompanying Fig. 2.

We shall see (Section 4) that surfaces with greater shear are more difficult to form; from eq. (10), this is related to the Gaussian curvature of the surface., are the fiber orientation.

3. CAD MODEL

Using an existing computer-aided-design software package, AutoCAD, several approximation algorithms were developed to create quick ways of visualizing the ideal mapping of fibers over arbitrary geometries, numerically calculating the in-plane shear, and predicting possible trouble spots for forming given parts.

The main components of this method are:

(a) A way to approximate the part geometry by describing it as a set of flat surfaces, joined by either radiused or sharp edges and corners,

(b) Algorithms to find ideal mappings of fibers over complex geometries and,

(c) Methods of calculating the amount of in-plane shear among fibers.

The accuracy of these approximation methods was tested by a set of numerical experiments. The methods were then tested over a range of complex parts.

Approximation Methods

Surface Generation

In order to create a fast algorithm to find fiber mappings, we described the surfaces to be mapped as a collection of flat faces joined by either sharp or rounded edges and corners. First, points on the actual part surface were chosen as vertices; then they were joined through either rounded or sharp edges that defined the flat faces. A hemisphere described by 16 flat facets and sharp edges is shown in Fig. 3.

Fiber Mapping

Ideal fiber maps, or the set of equally-spaced fibers required to form a specific part geometry, can be calculated once the part surface is properly described in the CAD system.

To determine such a map, first choose the orientation and placement of a single **initial fiber**. The position of all other fibers is then determined by the definition of ideal fiber placement. A geodesic path was chosen as the initial fiber path. When rounded edges are used, the initial fiber is chosen so that it will not go through corners, and follow a geodesic path across all edges. The fiber was continued across edges by using a algorithm that will be given.

Second, the initial fiber is offset by a user-specified distance, or **fiber spacing**, and redrawn onto the part surface.

Third, the second step is repeated until the desired area of the part was covered, or the edge of the part is reached.

Mapping over Edges and Corners

An algorithm was developed to map a fiber over an edge while maintaining ideal fiber placement.

Unless forced to shear in the plane, fibers will try to simply bend over an edge, maintaining zero in-plane curvature, i.e. following a geodesic path. If such a curve were to be developed into a flat plane, the fiber would trace a straight line, as shown in Fig. 4. Therefore, by geometry, the opposite angles α formed between the

fiber and the edge are equal. This property allows one to map a continuous fiber over two flat planes connected by a sharp edge.

On rounded edges, for a fiber to have no in-plane curvature, it has to follow a geodesic path over a section of a cylinder, that is a helix with the same pitch α as that determined by the fiber at the edge as of the flat (see Fig. 5).

Over corners, it becomes more difficult to analytically determine the fiber paths. However, in Fig. 5 we see that the effects caused by the double-curvature feature are bounded to a small area around the corner, shown by the dotted lines. The mapping of the fibers outside that small section is not affected by the fibers mapped over the corner. As will be seen, the effects caused by the rounded edges and corners can be further approximated and simplified without affecting the fiber mappings at a part scale, as long as the radii of curvature of those features remains small compared to the part scale.

Further Approximation Algorithms

We compared the mapping of fibers for cubes with rounded and sharp edges to quantify the effect of rounded features (Fig. 6) The same overall mapping and features appear in both rounded and sharp edge cubes (e.g..the position of the fiber which shears to π at a point). However, the sharp edge cube requires much less computation to plot the fiber mapping than the rounded cube.

The sharp-edged cube was compared with rounded cubes of varying radii of curvature edges and corners. The mappings did not change at the part scale, but the position of certain features did change slightly. The exact position of a specific

feature, the point where a fiber shears to π, was measured using the CAD program commands.

The difference in position of the chosen feature to a stationary point on the part between the sharp and each rounded-edge case was defined as the mapping error. The mapping error is proportional to the radii of curvature of the rounded features (see Fig. 7).

In cases where the rounded features are not small compared to the scale of the part, we first describe the curved surface as a series of flat faces connected by sharp edges. For example, a hemisphere was approximated by using 64 faces and fibers mapped onto it as shown in Fig. 8. (Only half of the sphere is shown mapped for clarity; the mapping is symmetrical about the center or initial fiber).

Numerical Experiments

Using the previoulsy described algorithm, ideal fiber maps were found for several surfaces for which ideal fiber mappings and in-plane shear were known, as well as more complex parts made up of combinations of simple geometrical features.

Numerically calculated shear values among the fibers were compared to theoretical expected values.

Shear Calculations

The lengths of the fibers from the ideal fiber maps for two different hemisphere approximations were measured and values of in-plane shear among fibers were calculated. The calculated values were compared to the theoretical values on Fig. 9. While both approximations did follow the expected values of shear, the accuracy of the shear values was dependent on the number of faces used. There exists a tradeoff between the accuracy of the calculated values and the complexity of the calculations required.

Singularities

Forming aligned-fiber composites into simple and complex geometries can sometimes generate undesirable features on the layout of the fibers. Mapped parts showed singularities (undesirable features in the fiber mappings) which we call **folds, cuts,** and **gaps,** which lead to part defects. Examples follow.

Folds are caused by the crossing of fibers onto themselves, violating the ideal fiber spacing, and in real processes, causing the material to fold. An example can be seen in Fig. 10. Some of the fibers on the right cube cross over themselves; at that point, a **fold** would occur in actual composite material. Folds occur when $\Gamma_{12} > \pi$.

Cuts occur on mappings where the fibers are required to shear to a magnitude of π at a point, as is the case on a side of the left cube on Fig. 10.

Gaps appear on fiber maps when several initial fibers are chosen, and the mapping then continued. In Fig. 11, two cubes on a flat plate were mapped by picking two initial fibers. As the mapping is continued, a gap develops where no

fibers are present. This would result in a hole or a thinner part section on actual parts.

To avoid singularities, one can taper the sides of a part, see Fig. 12.

4. OBSERVATIONS - FORMING EXPERIMENTS

Forming Apparatus

A room temperature diaphgram forming apparatus was constructed. This device, shown in Fig. 13 consists of an adjustable tool platform surrounded by a transparent PMMA tube. Prepreg preforms were placed between aluminum ring supported silicone rubber diaphragms, with petroleum gel being used as a lubricant. Forming operations were carried out by bolting the assembly together, and deforming the diaphragms and preform over the desired tool geometry by the application of positive pressure from the top and/or vacuum from beneath. The layered top cover of the apparatus incorporates a polycarbonate viewing window to allow deformation sequences to be studied. In this apparatus, the initial fiber is formed when the diaphgram just contacts the preforms and the tool.

Experiments

The sequence of experiments was as follows. Given part geometry and fiber orientation, net shape preforms were determined by back calculation from ideal fiber placement patterns. The preforms were placed between the silicone rubber diaphragms, oriented as necessary relative to the tool, and formed using positive

pressures of between 27.5 and 545 kPa. Pressurization rate was controlled manually by means of a ball valve and pressure gauge. Upon completion of forming operations, the parts were examined by removing the top diaphragm, the bottom diaphragm being held in place by the application of vacuum from beneath. A relaxation time of up to an hour was allowed to elapse before the part was removed from the tool, and measurements taken.

Hemispheres ranging in size from 1.9 cm to 15 cm in diameter were fabricated from two ply [0/90] preforms of AS4/3501-6 prepreg. 7.5 cm square boxes 2.5 cm deep were also formed with ply geometries of [0/90] and [± 45]. These figures show that the algorithm of Section 3 does in fact approximate how actual parts form.

The shear distributions for boxes and hemispheres with ideal fiber placements are shown in Fig. 17. Clearly, the build up of required in-plane shear relative to transverse distance from the central fiber is gradual on a hemisphere, whereas on boxes it occurs as a series of discrete steps.

Fig. 14 shows a 15 cm diameter [0/90] hemisphere formed over a 10 min time period. A [± 45] box formed in a similar time is shown in Fig. 15. In both cases the actual fiber mapping is similar to the ideal. An ideal mapping for a 45° ply on a box predicts that shear will be initiated along a line oriented at an angle to the top (initially contacted) face, the angle being simply half the lay-up angle. This line is indicated in Fig. 15. It is important to note that in-plane shear is not needed anywhere above this line. The edges of the box are formed by bending and torsion of the fibers.

The ideal fiber mapping for a hemisphere shows the occurence of a singularity at the edge of the part, where the final fiber is required to go through a shear of π. A similar situation occurs at the right most edge of the [±45] box shown in Fig. 15. In neither case is π shear achieved and in fact significant deviation from ideality is noted in fibers where the required in plane shear is significantly less. In the case of the box the *actual* line of shear development, gradually deviates from the predicted with increasing horizontal distance from the left most edge. This deviation which we term fiber misalginment, was evaluated by measuring the distance between ideal and actual fiber paths at the edge of the part, referenced to a central fiber which may be thought of as an "initially placed" fiber. On a hemisphere the reference is the fiber on the diameter, on a [±45] box it is the diagonal fiber, and on a [0/90] box it is the top fiber closest to the edge.

Correlation of Misalignment with Shear

Misalignment was measured for hemispheres varying in size from 1.9 to 15 cm diameter, and for boxes 7.5 cm square with lay-ups of [0/90] and [±45]. This group of shapes would appear to pose a broad array of forming problems. However, when the particular defect of misalignment is measured and related to an appropriate measure of shear, a clear pattern emerges. In Fig. 18 the misalignment (Δm) for all parts is shown to correlate closely with the integral of shear in the transverse direction up to the point of measurement. Thus the experimental data appears to fit a relation of the form

$$\Delta m = C_{p,m} \int_0^{s_n} \Gamma_{12} ds_n \qquad \text{(a)}$$

where $C_{p,m}$ is a constant dependent on the chosen process and material system.

5. CONCLUSIONS

Sections 2, 3 and 4 show that the formability of aligned fiber composites is a mapping problem. We have shown how differential geometry aids in describing the fiber paths, and most important, the fiber in-plane shear. The shear is related , by the Gauss Bonnet theorem, to the average surface curvature.

We also have developed a powerful algorithm, which correctly approximates the ideal fiber map. This algorithm is used to show typical geometric limitations of forming complex parts. We describe three such difficulties, cuts, folds, and gaps.

The model calculations do, infact, correspond approximately to observation, as the experimentally observed fiber placement is in approximate agreement with theory.

Finally, the integral of the in-plane shear is a convenient measure for the difficulty of achieving idea fiber placement.

REFERENCES

1. Pipkin, A.C., "Finite Deformations of Ideal Fiber-Reinforced Composites", in Analysis and Performance of Fiber Composites, Wiley, New York 1980, p. 251.

2. Pipkin, A.C., and Rogers, T.G., "Plane Deformations of Incompressible Fiber-Reinforced Materials", Transactions of the ASME, September 1971, p. 634.

3. Tam, A.S. and Gutowski, T.G., "The Kinematics of Forming Ideal Aligned Fiber Composites", *Composites Manufacturing*, Vol. 1, No. 4, Dec. 1990.

4. Struik, D.J., Lectures in Classical Differential Geometry, Dover Publications Inc., New York, 1988.

5. Tam, A.S., "A Deformation Model for the Forming of Aligned Fiber Composites", PhD Thesis, Department of Mechanican Engineering, Massachusetts Institute of Technology, June 1990.

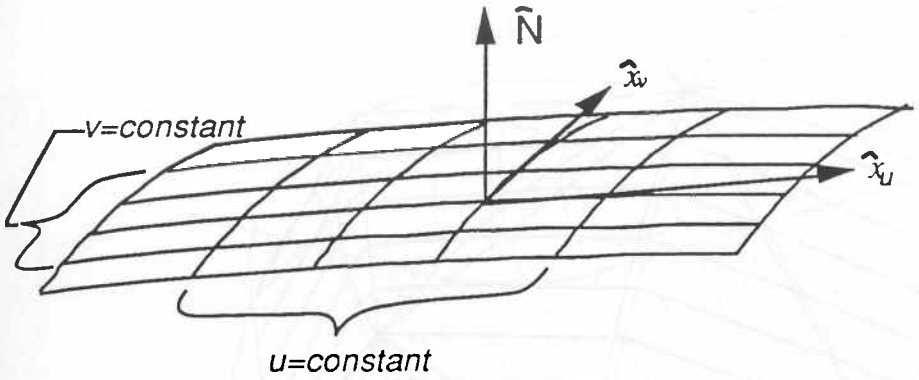

Fig. 1 Curved surface with tangent vectors and normal vector

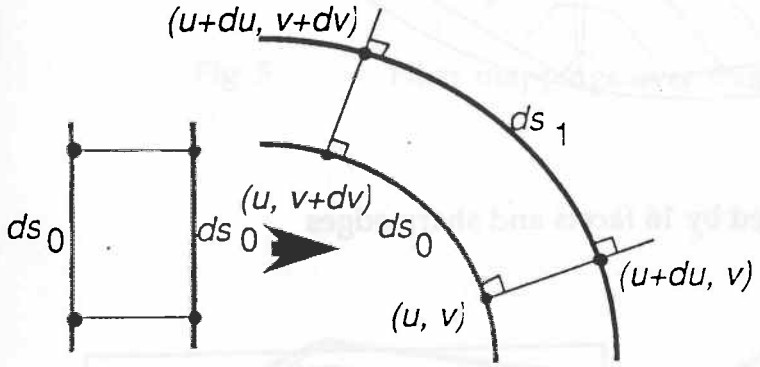

Fig. 2 Geodesic set on a plane sheet and a surved surface

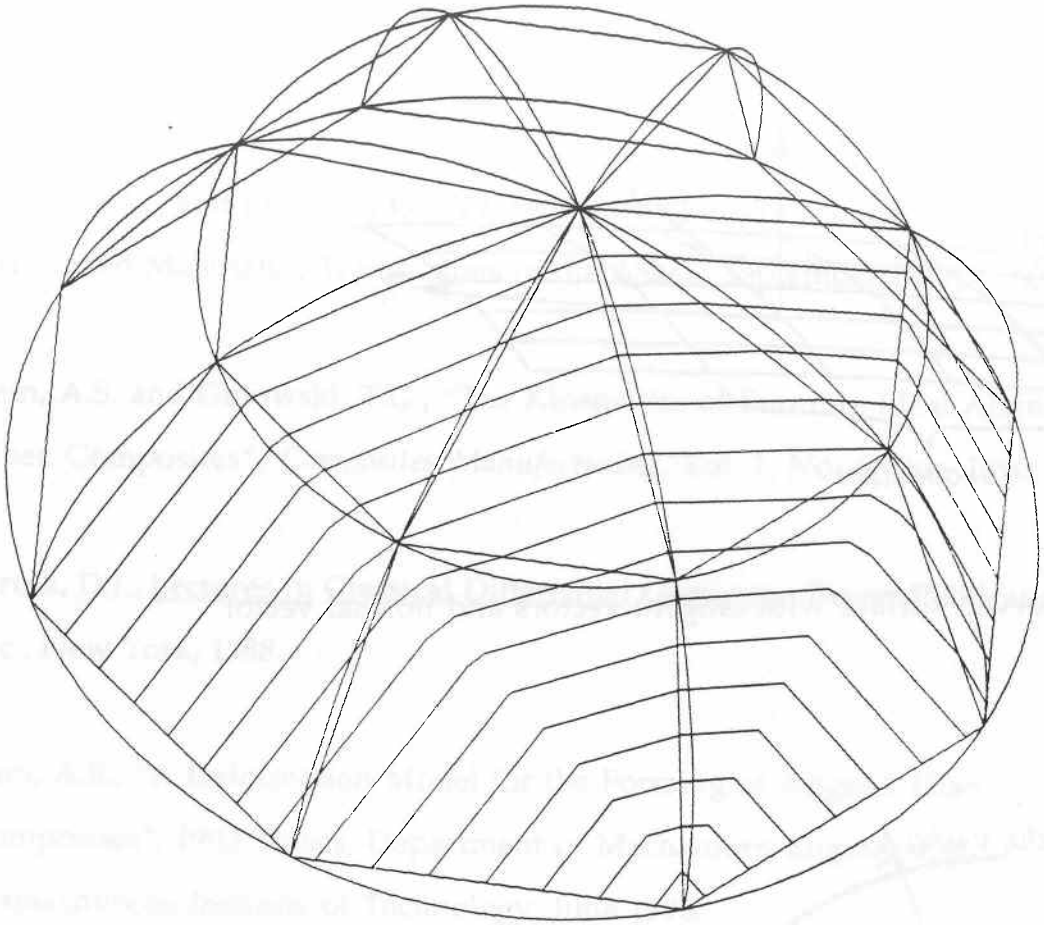

Fig. 3 Hemisphere described by 16 facets and sharp edges

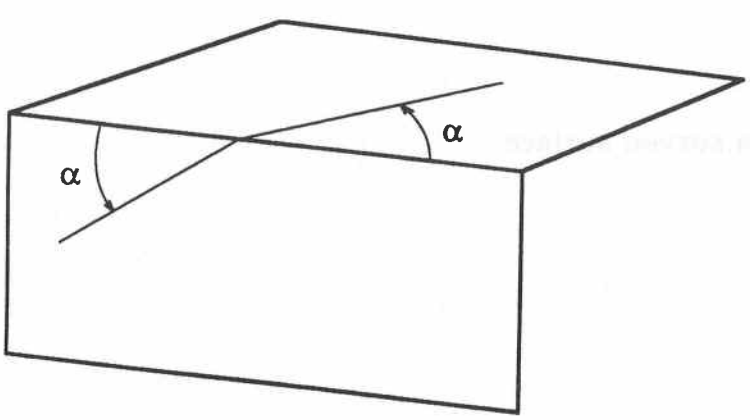

(a)

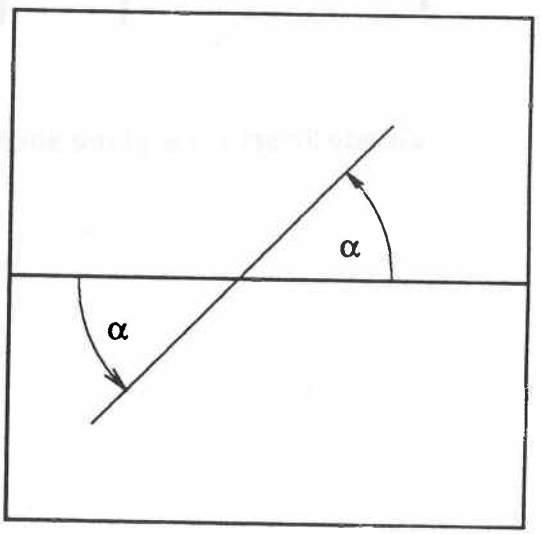

(b)

Fig. 4 (a) A line following a geodesic path over an edge (b) when developed into a flat plane it traces a straight line.

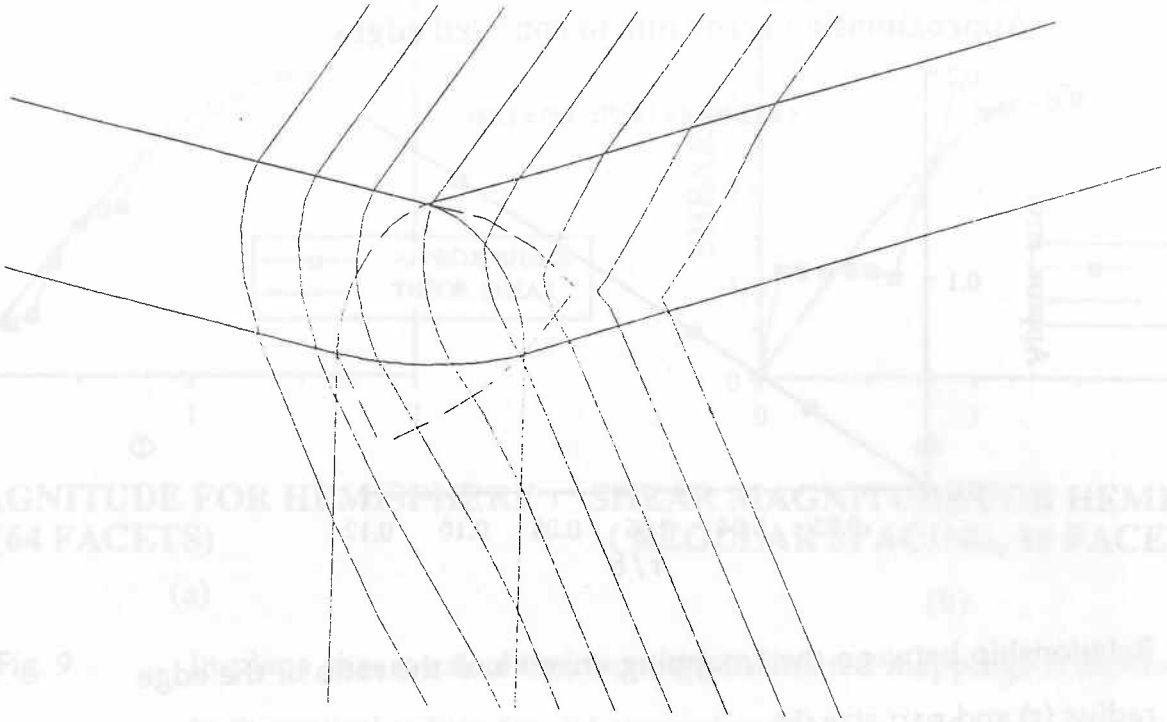

Fig. 5 Fiber mappings over rounded edges and corners

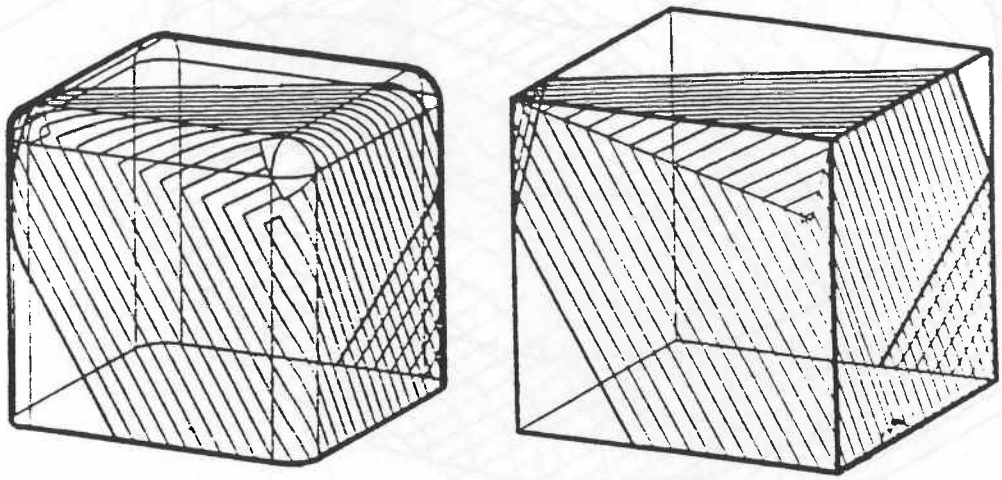

(a) (b)

Fig. 6 Fiber mappings over (a) a rounded edge and (b) a sharp edged cube.

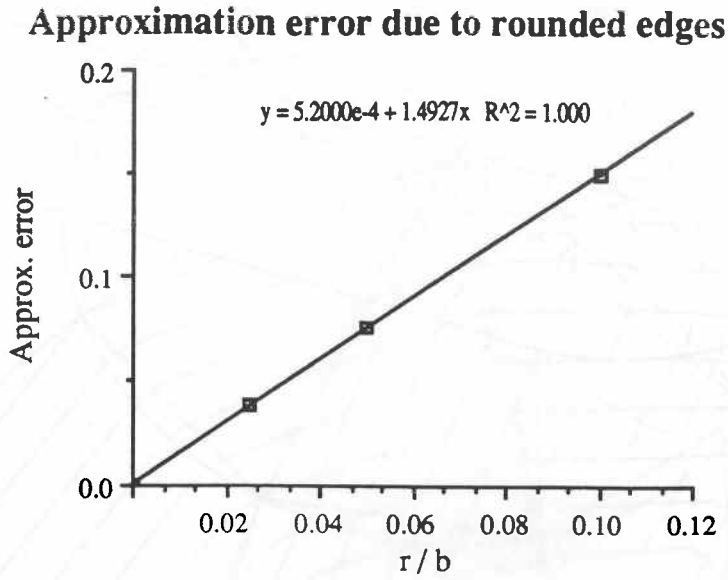

Fig. 7 Relationship between the "mapping error" and the ratio of the edge radius (r) and part size (b).

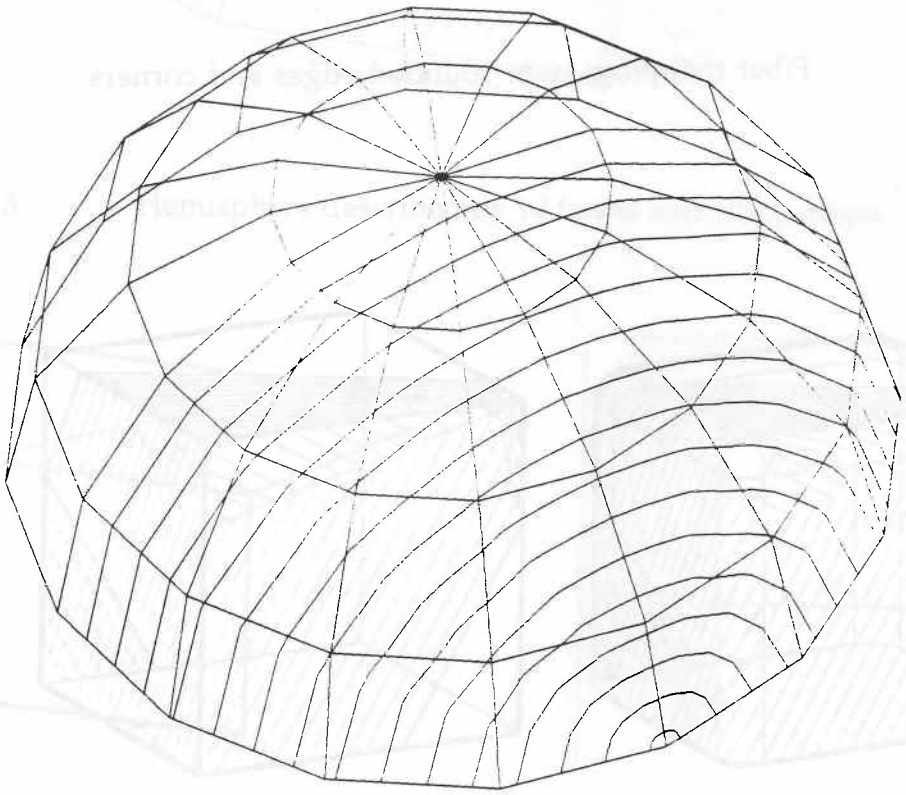

Fig. 8 Approximation of a hemisphere fiber mapping using 64 flat facets

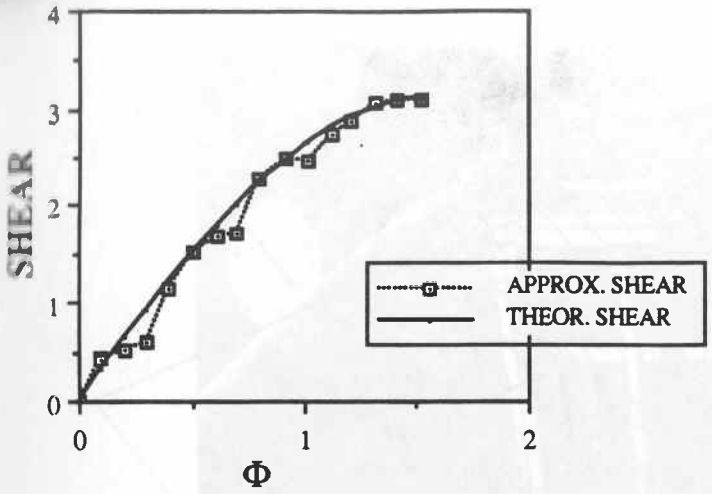

AR MAGNITUDE FOR HEMISPHERE
(64 FACETS)

(a)

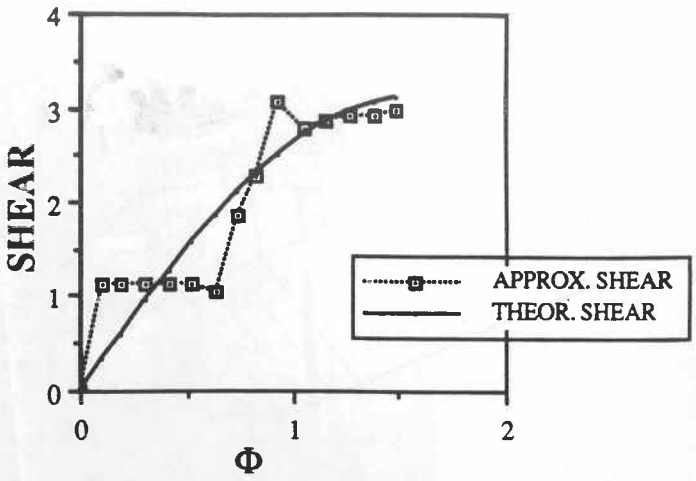

SHEAR MAGNITUDE FOR HEMISPHERE
(REGULAR SPACING, 16 FACETS)

(b)

Fig. 9 In-plane shears calculated from approximated mappings compared to theoretical values for (a) approximation using 64 facets and (b) approximation using 16 facets.

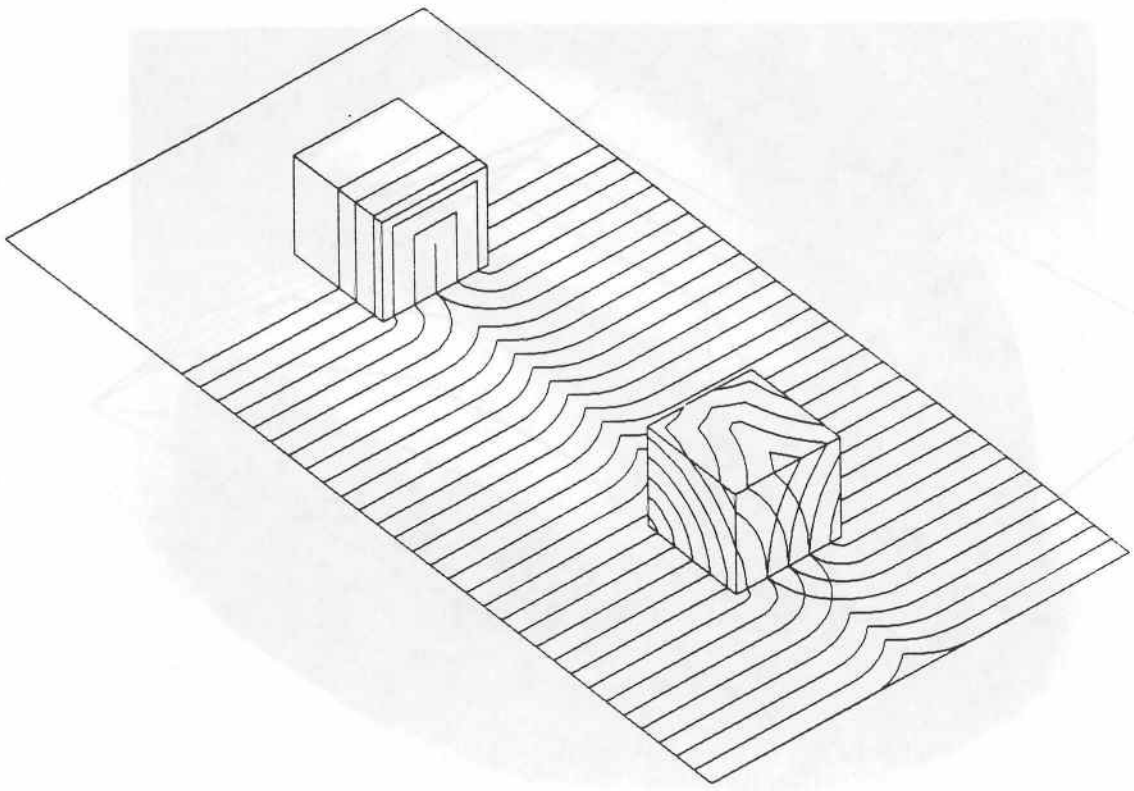

Fig. 10 Illustration of occurence of singularities referred to in text as cuts (top box) and folds (lower box).

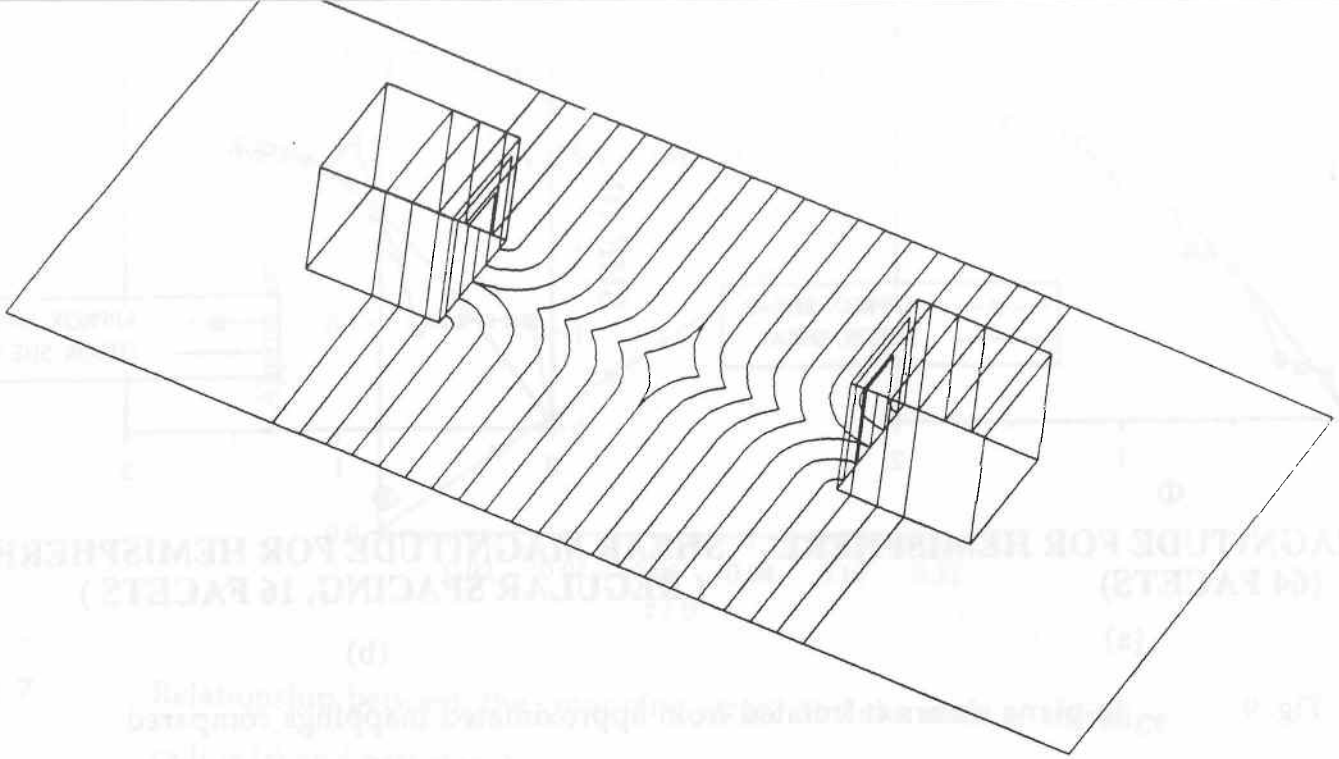

Fig. 11 Illustration of development of gaps where fiber mappings are propagated from initially placed fibers in different locations.

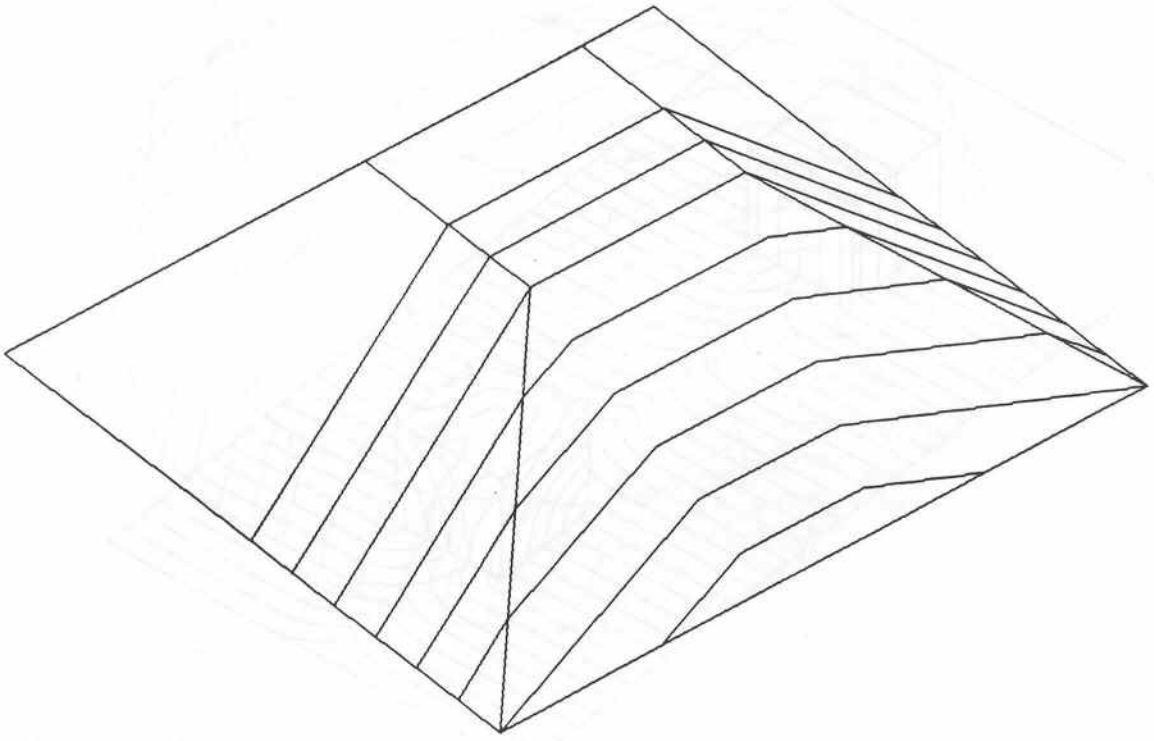

Fig. 12 A box with tapered sides does not develop singularites in the fiber mappings.

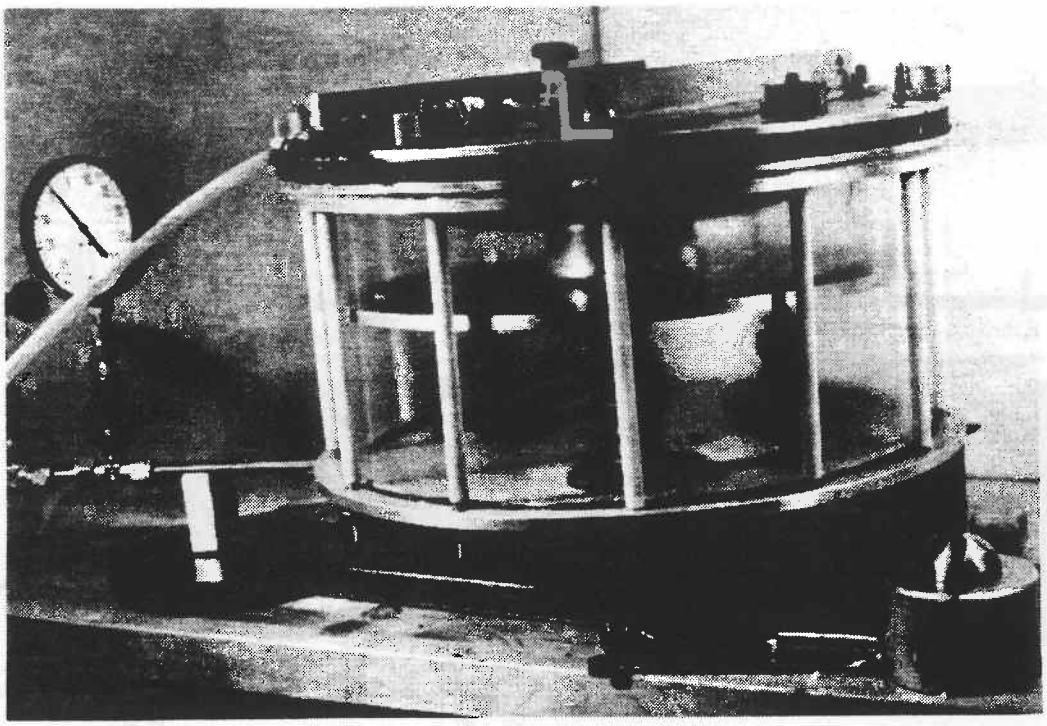

Fig. 13 Room temperature diaphragm forming apparatus.

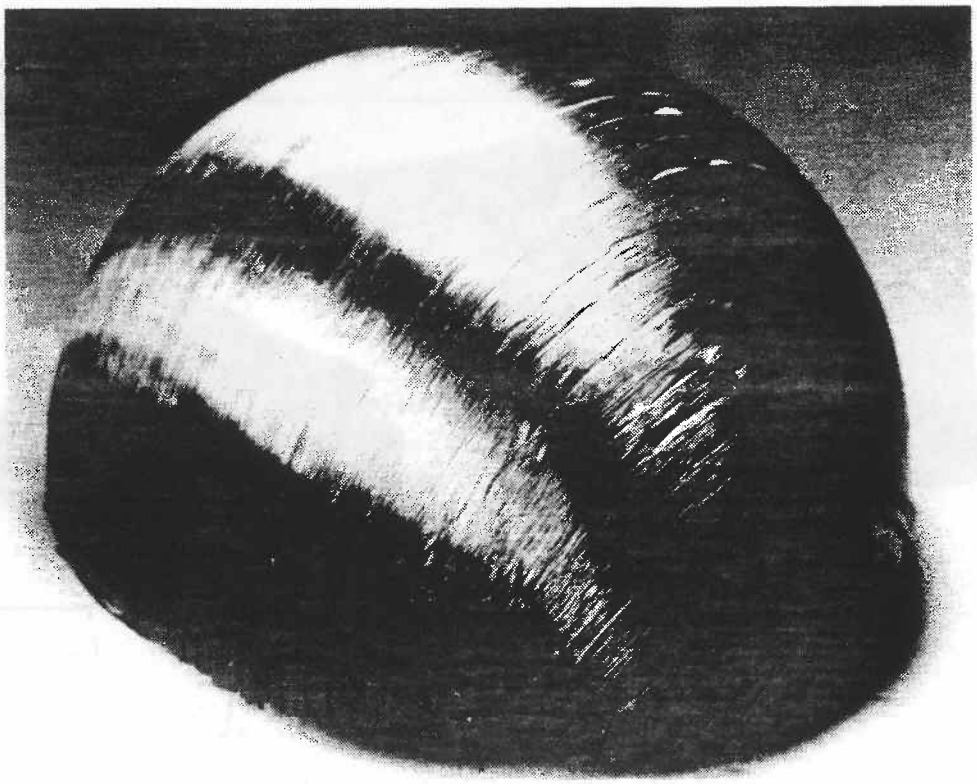

Fig. 14 15 cm. diameter hemisphere formed at room temperature.

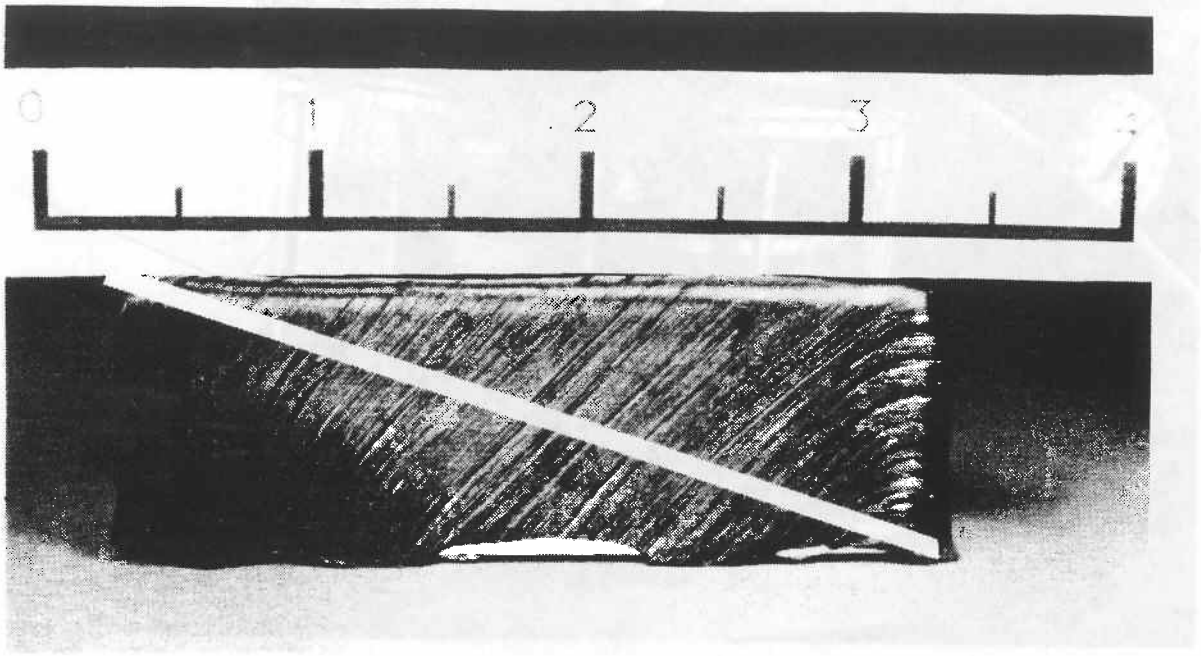

Fig. 15 7.5 cm square box formed with (±45°) ply orientation.

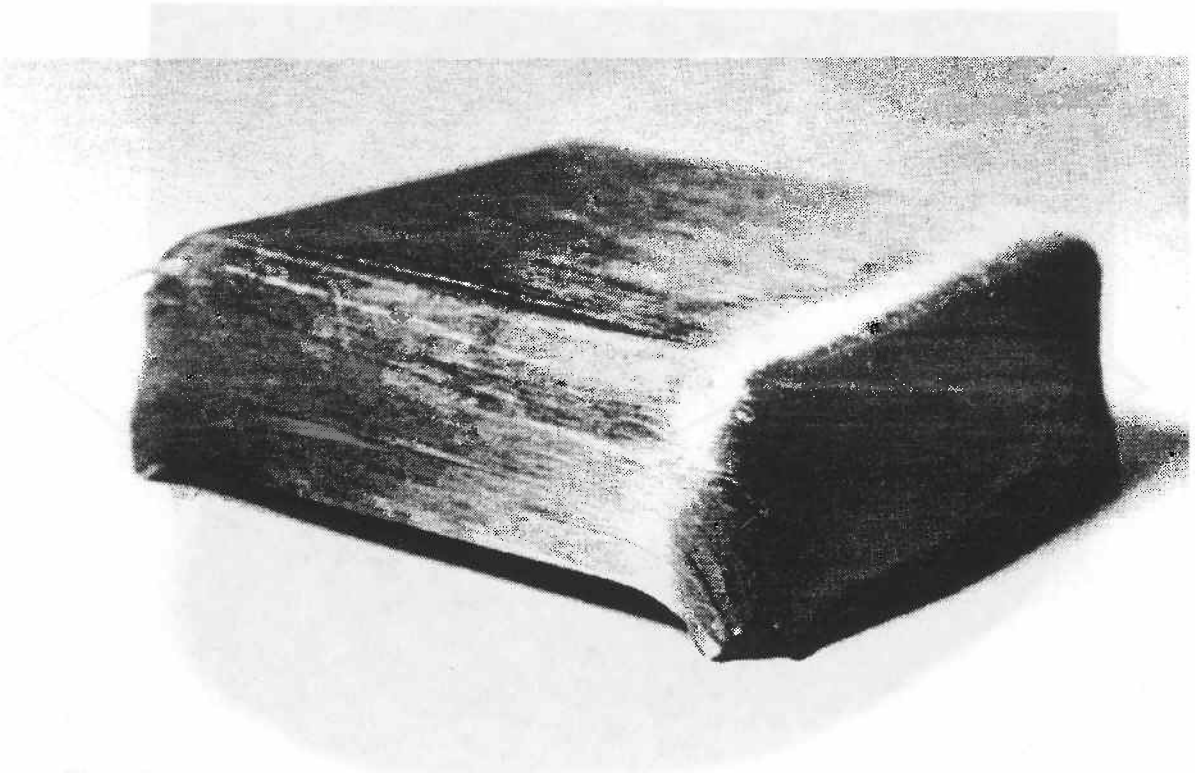

Fig. 16 75 cm. square box formed with (0°/90°) ply orientation.

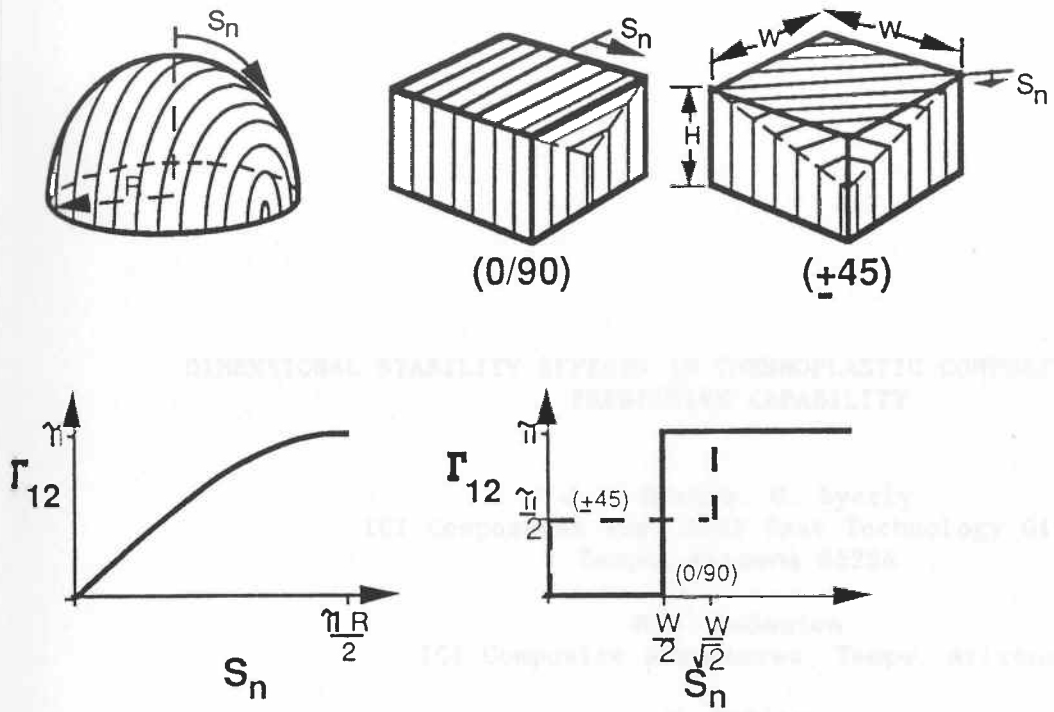

Fig. 17 Fiber patterns and shear distributions for boxes and hemispheres

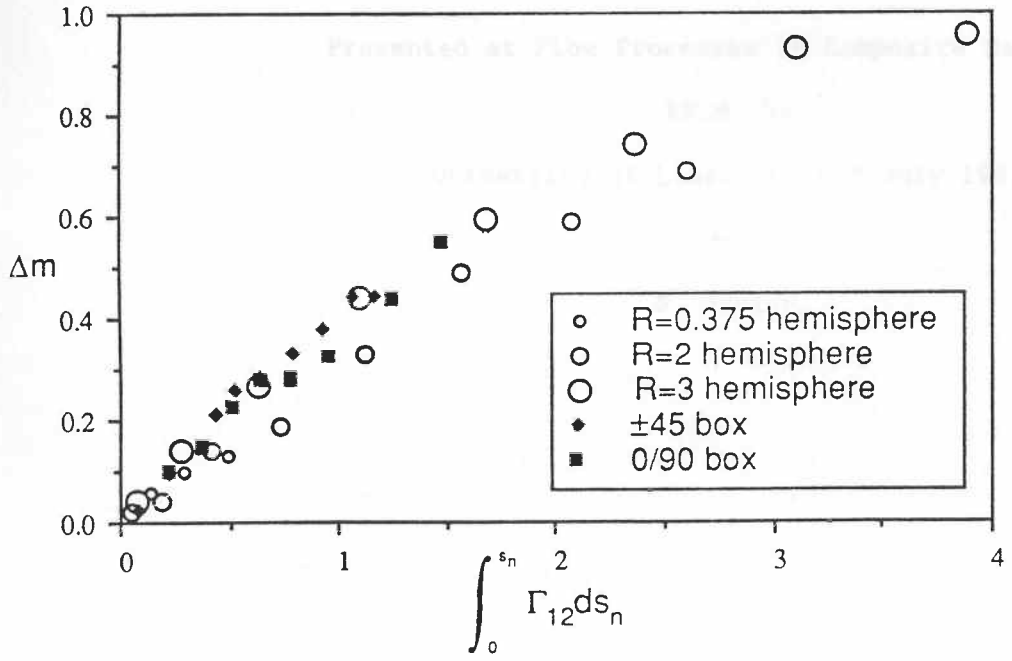

Fig. 18 Experimental forming data for boxes and hemispheres.